

Phd. Mihail Lungu

**MICRO-ANALYSIS TECHNIQUES
FOR PLASMA FACING COMPONENTS**

**Editura Academiei Oamenilor de Știință din România
București, 2019**

Acknowledgments

“This work has been carried out within the framework of the EUROfusion Consortium and has received funding from the Euratom research and training programme 2014-2018 under grant agreement No 633053. The views and opinions expressed herein do not necessarily reflect those of the European Commission.”

Descrierea CIP a Bibliotecii Naționale a României

LUNGU, MIHAIL

Micro-analysis techniques for plasma facing components / Mihail Lungu. -

București : Editura Academiei Oamenilor de Știință din România, 2019

Conține bibliografie

ISBN 978-606-8636-61-0

Table of content

Chapter 1. Introduction.....	11
Chapter 2. Fusion reactions and reactors	13
2.1 Fusion reactions	13
2.2 Fusion reactors and functional materials.....	15
Chapter 3. Applied analysis methods.....	20
3.1 Alternative analysis methods	21
3.1.1 Glow discharge optical emission spectroscopy method	21
3.1.2 Scanning electron microscope method	22
3.1.3 Rutherford backscattering method	23
3.2 Non-destructive methods	24
3.2.1. X-ray sources.....	25
3.2.2 The generation principle of X-ray fluorescence.....	27
3.2.3 Optical concentrator elements.....	29
3.2.4 X-ray detectors and spectra analysis protocols.....	31
Chapter 4. X-ray fluorescence-based analysis methods	38
4.1 Low energy X-ray fluorescence method.....	38
4.2 X-ray fluorescence at high energies (K-lines)	42
4.3 Numerical simulation of fluorescence spectra.....	43
Chapter 5. Calibrations and optimizations conducted on methods developed in the micro-tomography laboratory	45
5.1 Steps required for calibration and validation of X-ray fluorescence methods	45
5.2 Standard sample calibration.....	46
5.2.1 Thin layers deposition by means of the TVA method.....	46
5.2.2 Spatial distribution of the concentration of elements deposited by the TVA method.....	49

5.3 Calibration of X-ray fluorescence methods by standard samples.....	53
5.3.1 Calibration of the X-ray micro-fluorescence method	53
5.3.2 Validation of the spatial resolution of the X-ray micro-fluorescence investigation method.....	56
5.3.3 Calibration of the X-ray fluorescence method at high energies.....	59
Chapter 6. Monte Carlo simulations applied in X-ray production and transport processes	61
6.1. Determination of matrix effects correction factors	63
6.2 Monte Carlo simulations regarding the fluorescence signals for elements relevant to the inner wall of tokamak reactors	67
Chapter 7. Experimental results	70
7.1 Relevant and unexposed samples to fusion plasma	70
7.1.1 Complex characterization of PFC relevant samples	70
7.1.2 Complex characterization of the Be, C, W samples deposited using the TVA method	74
7.2 Analysis of the samples exposed to tokamak plasma fusion	79
7.2.1 Study of the physical phenomena of plasma and material interaction occurring inside the fusion reactor	80
7.2.2 Analysis of fusion plasma exposed samples	82
7.3 Comparative analysis before and after exposure to fusion plasma of marker lamellae surface.....	84
7.3.1 Experimental data processing	88
7.3.2 Monte Carlo simulations of X-ray fluorescence response for witness samples measurements	91
7.3.3 Discussing the experimentally determined results	94
Conclusions	101
References	104

List of abbreviations

TVA	Thermionic vacuum arc
CMSII	Combined magnetron sputtering with ion implantation
XRF	X-ray fluorescence
NILPRP	National Institute for Lasers, Plasma and Radiation Physics
GDOES	Glow discharge Optical Emission Spectroscopy
SEM	Scanning electron Microscope
RBS	Rutherford back-scattering spectroscopy
Micro-XRF	Micro X-ray Fluorescence
HEXRF	High Energy X-ray Fluorescence
QCM	Quartz crystal microbalance
ITER	International Thermonuclear Experimental Reactor
JET	Joint European Torus
PFC	Plasma Facing Components
ASDEX	Upgrade Axially Symmetric Divertor Experiment-Upgrade
CFC	Carbon fibre Composites
DEMO	DEMONstration Power Station
EDS	Energy dispersive spectroscopy
XRD	X-ray diffraction
FWHM	Full width at half maximum
FPGA	Field Programmable Gate Array
XCT	X-ray tomography
FP	Fundamental Parameter
CMOS	Complementary metal-oxide semiconductor
TEM	Transmission electron microscope
ILW	ITER like wall
PWI	Plasma wall interactions

List of figures

Figure No.	Figure Title
2.1.1	Internal overview on a tokamak type fusion reactor (ITER)
2.1.2	Plasma-wall interaction overview
2.1.3	Cross section-temperature dependence for D-T, D-D respectively D-3He
2.2.1	The currents and the magnetic fields in the produced plasma in a tokamak reactor environment
2.2.2	Poloidal cross section (ITER)
3.1.1	Working principle of the GDOES method
3.2.1	Characteristic spectra of W target X-ray source
3.2.2	Source configurations with stationary another at tilted angle (left) and transmission type source (right)
3.2.3	Schematic representation of the X-ray fluorescence principle
3.2.4	Advantages of the concentrating lens configuration when compared to the collimated and non-collimated source
3.2.5	Full width at half maximum (FWHM) in an experimental spectrum;
3.2.6	GUI of MCA software for acquired spectra by means of Si-pin detector
3.2.7	Differences between the real time and the acquisition time [45]
3.2.8	The conversion between detector channels and energy [keV]
3.2.9	Fitting parameters by means of Gaussian function
3.2.10	ADMCA user interface
3.2.11	Gaussian integration of W L-lines
4.1.1	Tomo-Analytic facility components
4.1.2	Components of the micro-XRF method
4.1.3	X-ray sources integrated in the Tomo-Analytic instrument
4.1.4	The working principle/configuration of the X-ray transmission method
4.1.5	X-ray fluorescence spectra interpretation and Compton scattering
4.2.1	HEXRF experimental configuration
5.1.1	Calibration procedure and deposition study diagram
5.2.1	Single anode-cathode experimental configuration of the TVA method
5.2.2	Three anode-cathode experimental configuration of TVA method
5.2.3	Deposition geometry by means of TVA method
5.2.4	Schematic configuration of TVA method in configuration with three pairs of anodes and cathodes (A1, A2 and A3)
5.2.5	Comparison of spatial distribution of layers deposited both in fixed geometric configuration and in rotational symmetry
5.2.6	Variation of deposit uniformity dependent on the height of the anode position

- 5.2.7 Variation of deposition uniformity dependent on the height of anode position (h) at extreme values
- 5.2.8 Variation of deposit distribution dependent on the distance between the electrodes projection and the centre of the sample holder
- 5.3.1 Influence of the W thickness layer on the shape of the spectrum in energetic intervals of $WL\alpha$ and $WL\beta$
- 5.3.2 Calibration curve determined from thin layer W samples (<50 nm) deposited on C and Si substrates
- 5.3.3 Calibration curve determined based on samples deposited with W on C and Si
- 5.3.4 Calibration curve for Ni layers deposited on C, Si and glass respectively (a); Linear behaviour of the area integrated values in relation to the studied layer thickness regarding very thin layers (b)
- 5.3.5 Image captured by the CMOS flat panel detector of the collimated beam by polycapillary lens in optimal alignment configuration
- 5.3.6 Micro-XRF line profiles for a Cu grid
- 5.3.7 Micro-XRF line profile for a Pbgrid with 50 μm step
- 5.3.8 Linear micro-XRF profiles for 25 μm Pb grid
- 5.3.9 The spectra of two Ti substrate calibration samples (red and blue) and a C substrate based sample (black)
- 5.3.10 Calibration curve converting W K-line intensities to layer thicknesses
- 5.3.11 HEXRF analysis applied on the calibration samples deposited by CMSII (layer thicknesses are relatively close to hundreds of nm) (a) [50]. Dependency curve between integrated fluorescence lines and layer thicknesses (b)
- 6.1 Diagram of successive step for cross sections library definitions
- 6.1.1 Highlighting the matrix effects producing amplifications in the alloy intensity (a) and attenuation (b)
- 6.1.2 Spectrum intensity comparison for the Ni-W alloy with pure Ni
- 6.1.3 Variation of Fe, W, Cr depending on the order of deposition of layers
- 6.1.4 The intensity ration do not depend on the thickness of the elements
- 6.2.1 Overlapping the experimental with the simulated curves for W (a) and Ni (b)
- 6.2.2 Monte Carlo simulation of WK line intensities at different X-ray generator working voltage values
- 6.2.3 Simulated curves for the L (a) and K (b) lines of Mo on the Si substrate determined by the excitation source with anode W (a) and Cu anode (b)
- 7.1.1 Image with the analysed samples and the deposition configuration with dimensions for the samples mounted on the sample holder
- 7.1.2 Spatial distribution of deposition conducted in 3 anodes fixed geometry
- 7.1.3 Micro-XRF linear profile of reference samples

- 7.1.4 Empirical and theoretical spatial distribution for Ni thickness determined by means of studying the samples deposited in the fixed geometry configuration
- 7.1.5 Theoretical data and experimental points with and without matrix effects corrections applied to the characteristic lines of Ni
- 7.1.6 Atomic concentrations distribution for the W, Fe and Ni expressed for samples deposited in fixed geometry configuration
- 7.1.7 Indexing co-deposited samples with Be, C, W in fixed geometry and rotational symmetry
- 7.1.8 Integration of peak of interest ($W_{L\alpha}$, $L\beta$) and background noise extraction from the fluorescence spectrum
- 7.1.9 W thickness distribution expressed in nm and at/cm^2 for Be, C, W alloys (rotated geometry) relative to the distance of the samples from the centre of the sample holder
- 7.1.10 Spatial distribution of W expressed in atomic mass concentrations on Be, C and W samples in the fixed geometry configuration
- 7.1.11 a. W thickness distribution (at/cm^2) from W to Be anode projections; b W thickness distribution (at/cm^2) from W to C anode projections; c W thickness distribution (at/cm^2) from the projection between W-Be towards the C projection; d W thickness distribution (at/cm^2) from Be to C anode projection
- 7.1.12 Experimental RBS spectrum of a sample of Be, C, W overlapping the spectrum simulated by the SIMRA program
- 7.1.13 a W concentration (at/cm^2) from W to Be anode projection; b W concentration (at/cm^2) Be to C anode projection
- 7.1.14 Results comparison between the RBS and micro-XRF + errors (at/cm^2)
- 7.2.1 Several enumerated processes involved in plasma-wall interactions
- 7.2.2 XRF spectrum on calibrated W-Fe/Ti sample and the experimental configuration
- 7.2.3 The fluorescence spectra of the exposed samples extracted from the divertor
- 7.2.4 XRF measurements in relation to the spatial distribution of samples in the divertor area
- 7.3.1 Layer deposition order on the witness lamellae
- 7.3.2 Localization of witness lamellae in the divertor area
- 7.3.3 XRF experimental configuration; mounting position of W/Mo lamella
- 7.3.4 HEXRF line profile on a SS grid
- 7.3.5 a) The fluorescence spectrum acquired from a witness sample; b) Area integration on characteristic energy intervals for W ($L\alpha$, $L\beta$); c) Area integration for the Mo K α characteristic energy line
- 7.3.6 Intensity ratio $\text{Mo}(K \text{ line})/\text{W}(L \text{ line})$ for unexplained plasma fusion samples

- 7.3.7 Mo/W variation at different integration time measurements
- 7.3.8 Reports of Mo(K line)/W(L line) for exposed samples; samples with a strong variation of the integrated signal areas are marked in red
- 7.3.9 Measurements on samples with strong Mo/W ratio variations
- 7.3.10 The exposed/non-exposed ratio for W exhibits a higher probability of erosion than redeposition
- 7.3.11 Investigated area on sample A22
- 7.3.12 Mapping the intensities of the characteristic lines of W (a) and Mo (b), respectively, on the investigated surface
- 7.3.13 Comparative study between different energetic lines
- 7.3.14 Simulation of M.C. of the continuous energy spectrum for the W anode source
- 7.3.15 Simulated geometry configuration for the XRF applied method
- 7.3.16 The calibration curve that correlates the W layer thickness with the Mo/W intensity ratio
- 7.3.17 Substrate influence on simulated fluorescence intensities of Mo and W
- 7.3.18 An in-depth profile of deposition witness samples by means of GDOES method
- 7.3.19 Linear profile on the Mo/W ratio variation by means of XRF method applied on deposition witness samples
- 7.3.20 Cross section SEM image on the deposition witness sample
- 7.3.21 Corrected calibration curve by means of correction factors and comparison with experimental point determined by means of GDOES method
- 7.3.22 Linear profiles of deposited W layer measured on non-exposed (left) and plasma exposed (right) lamellae
- 7.3.23 Thickness profiles on W layer (at/cm²)
- 7.3.24 Experimental data comparison between data determined by means of RBS and XRF methods

List of tables

Table 2.1	Relevant parameters for the most used materials in the fusion reactors [13]
Table 3.1	Relevant samples used in the fusion technology, characterised by means of different analysis techniques
Table 6.1	Matrix coefficient determination for W-Ni alloy and bulk W
Table 6.2	Matrix coefficient determination for Fe-Ni alloy and bulk Fe
Table 7.1	Visual investigation on exposed samples by means of digital microscope
Table 7.2	Correction factor determination
Table 7.3	W thicknesses determined by means of XRF and RBS methods

Chapter 1. Introduction

The development of the society is strictly dependent on energy obtaining methods. However, the energy obtaining process is intended to be realized through methods that are less destructive, for example, through the reduction of CO₂ emissions into the atmosphere. Although massive investments were made to develop alternative ways of producing ecosystem friendly energy, these methods are currently applied at low scale. Therefore, the interest in finding new ways to obtain and conserve energy has evolved in the past decade in the science field [1].

This work focusses on the nuclear power plants that work on fusion, an alternative that is more reliable in the long term when compared to fission power plants.

The nuclear power plants determine an energy conversion from the reactions that happen at the atomic scale. The heat generated as a result of the fusion reaction is extracted through a system that generates steam and rotates a turbine that is connected to an electrical energy generator [2]. The exploration into the nuclear fusion industry started in 1940. This subject is interesting because of the low toxic emissions into the atmosphere and lack of radioactive waste, such as in the fission reactors [2].

The main advantages of applying fusion energy when compared to the conventional fission energy are the good impact on the environment, the lack of radioactive waste from the nuclear reactions and a high yield of process that was determined from the ratio between the input energy for maintaining the fusion plasma in stationary state and the determined output energy.

In the past few years, an exponential increase in interest was observed in the nuclear fusion energetic domain. This led to the development of materials applied as plasma facing components. Functional materials are widely applied in the nuclear domain as erosion marker lamellae in the reactor walls that are directly exposed to the fusion plasma or in the industry domain, such as depositions with high resistance to high temperatures.

Currently, the material optimisation included in the reactor vessel is a topic of much interest. Therefore, the formation of nuclear radioactive waste and a reduction of the erosion processes such as the erosion, re-deposition and melting of constituents elements are intended to be avoided. The enumerated phenomena are determined based on the fact that the plasma confinement process is not perfectly stabilized [2].

The primary aim of the current work is the study of erosion, re-deposition and transport phenomena on the elements that are included in the tokamak type reactor walls, which are present during the plasma ignition. The majority of applied investigation equipment is present and some of them have been built in the National Institute for Plasma, Lasers and Radiation Physics.

The main purpose of this work is to study the erosion, deposition and transport phenomena of the relevant elements used as plasma facing components in the tokamak type reactors. Plasma relevant layers were prepared with those found on the first wall of the reactors, made of pure and mixed materials. Some of the applied techniques are the in-house methods as the thermionic vacuum arc (TVA), the combined magnetron sputtering with ion implantation (CMSII) and X-ray fluorescence (XRF), techniques that were developed at the National Institute for Lasers, Plasma and Radiation Physics (NILPRP).

This paper contains a total of 8 chapters; each chapter has been structured in subsections based on the complexity of the studied subject.

Chapter 2.

Fusion reactions and reactors

In **Chapter 2**, the doctoral research motivation is mentioned that relies on a complex research field that includes the reactions and reactors relevant in the fusion plasma domain. The objective of the thesis relies on the surface microanalysis of relevant samples in order to obtain possible solutions on a wide variety of problems that limits the fusion power plants from being commercially available. Therefore, the current study aims to calibrate and validate the protocol of a non-destructive investigation method, namely the XRF method, in order to apply it on plasma facing components.

2.1 Fusion reactions

At the base of producing nuclear fusion energy is the reaction between two low atomic mass nuclei that favour the formation of a nucleus of a higher atomic mass; this process results in an energy output. Each nuclear reaction is unique and is characterized by an energetic yield Q and a cross section σ dependent on the energy. The cross section represents the probability of overcoming the Coulomb threshold after the fusion reaction takes place [3].

The reaction that takes place inside the reactor has to have cumulated conditions such as exothermal reactions ($Q > 0$) and high values for the cross section at relevant high energies. This was achieved using a hydrogen isotope, such as Tritium and Deuterium [4].

The primary advantage of producing the fusion energy is the high yield, determined based on the ratio between the energy output in relation to the input energy responsible for maintaining the fusion in a stationary state ($Q = E_{\text{output}}/E_{\text{input}}$). In particular, for the ITER future reactor (International Thermonuclear Experimental Reactor), this ratio is expected to be around 10 [4]. The ITER reactor will be built in a tokamak configuration (Figure 2.1.1).

A particular case for obtaining the fusion energy is shown by the exothermic reaction between D and T. The result of the reaction is the He atoms (^3He), a neutron (n) and a massive energy production. Under fusion reactions, high values of energy of 14 MeV are produced and, therefore, resistant materials need to be used as plasma facing components in order to withstand high power fluxes and temperatures [6].

The value of 14 MeV is one order of magnitude higher than the mean energy produced using conventional fission reactors. This high value determines the production of a high number of intermediate products, for example ^3He , that are retained in the reactor walls and can, in time, cause an alteration in the mechanical properties of the fusion reactor walls and the quality of the reaction [7].

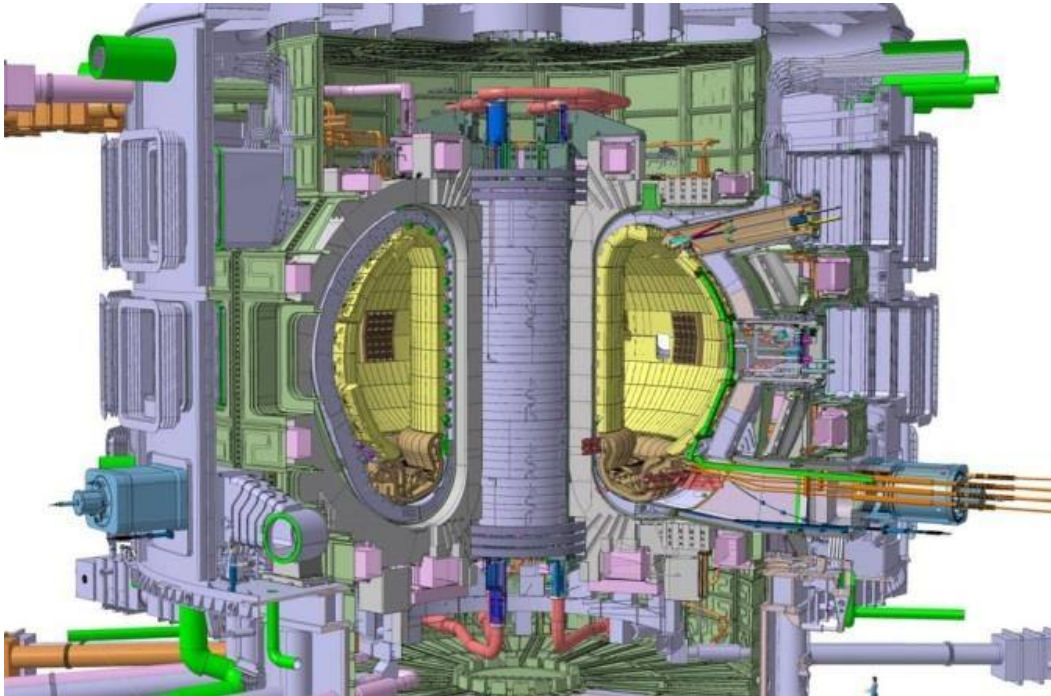


Fig. 2.1.1 *Internal overview on a tokamak type fusion reactor (ITER) [5]*

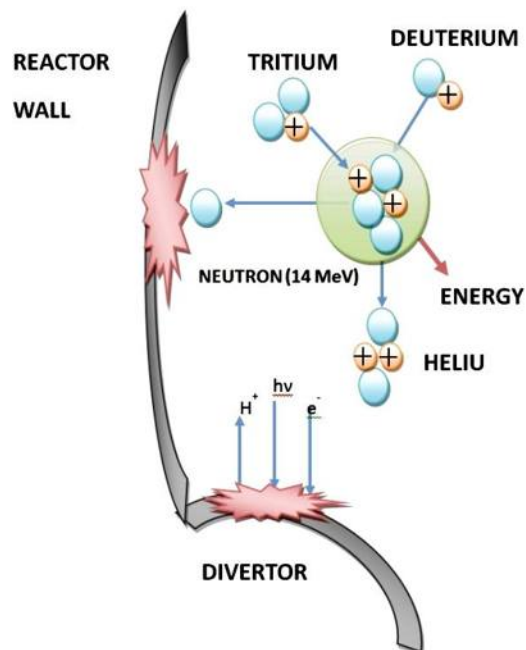
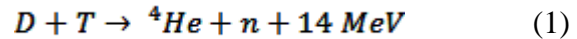


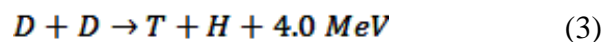
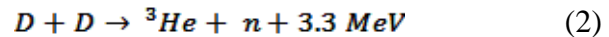
Fig. 2.1.2 *Plasma-wall interaction overview*

The D and T reactions are the most proper as the emergent particle energy is proportional with the mass. Taking into account the ${}^4\text{He}$ alpha particle, the D-T reactions could be expressed such as:



where He^4 represents the He isotope that is an alpha particle, and n is the neutron [8].

Other reactions that involve the use of D isotope and have the same rate of production are:



respectively, where H represents the proton. The energy produced from the reaction represents the total output energy. Thus, this is the kinetic energy of the reaction [8].

The alpha particle positively charged and produced after the D and T reaction remains confined and transport its energy through the fusion plasma. The energetic neutrons escape from the plasma volume; however, at the same time, their energy is converted by means of a complex system in heat and finally in electricity [8].

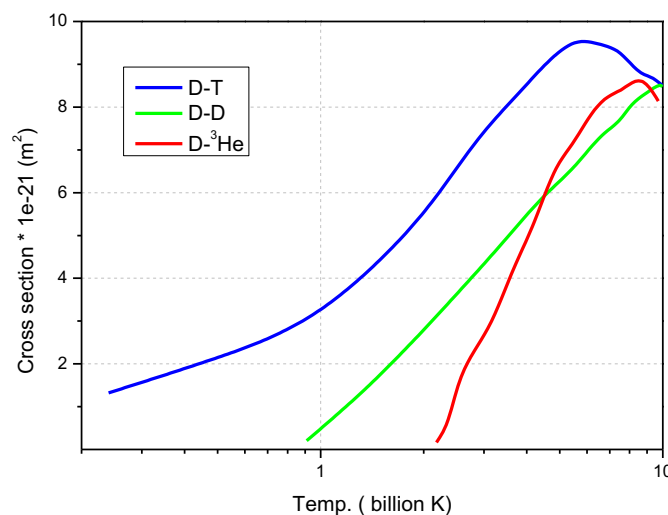


Fig. 2.1.3 Cross section-temperature dependence for D-T, D-D respectively D- ${}^3\text{He}$ [8]

For the applicability in fusion, the cross section of D and T is sufficiently high only at high energies. Therefore, extreme temperatures over 100 million K are necessary in order to obtain nuclear fusion reactions (Figure 2.1.3) [8].

2.2 Fusion reactors and functional materials

For example, due to the Sun's mass, the particles that are at high temperatures up to 100 million K are held together through the existent gravitational force. In the

absence of the gravitational force, the particles would scatter at very high velocities. Therefore in an terrestrial reactor, particles with the mentioned velocities would interact with the near vicinity chamber walls in under millisecond time [9].

One solution for the production of fusion reactions on Earth is given by the tokamak configuration reactors. These reactors work on the confinement principle under the action of a toroidal and poloidal type electromagnetic field [10]. The fusion reactions that involve the use of hydrogen isotopes are produced at low pressure in the confined plasma as a result of the action of supra-conductor coils [5].

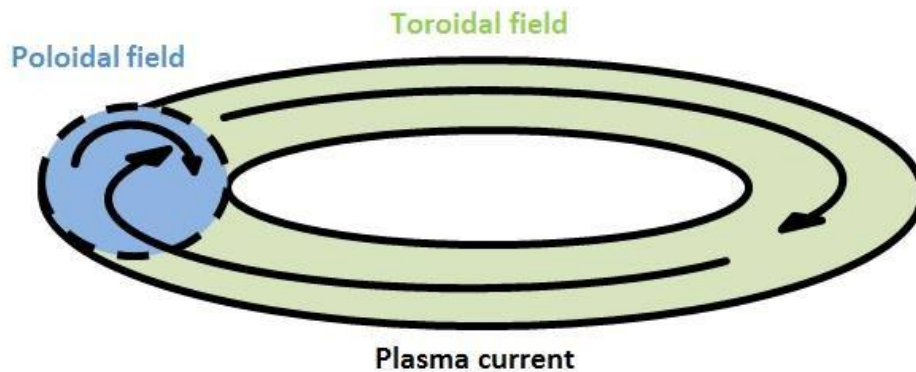


Fig. 2.2.1 The currents and the magnetic fields in the produced plasma in a tokamak reactor environment

The fusion reactions that show the use of hydrogen isotopes are produced at low pressure in a plasma discharge that is confined under the action of magnetic coils constructed from supra-conducting materials [11].

Since 1983, the Joint European Torus (JET) from Culham UK has been the biggest and most powerful fusion reactor in the world with a tokamak type configuration. This reactor has the capability to work with a D-T mixture of nuclear fuels. Inside the reaction vessel, the confinement of the plasma is maintained by application of the toroidal and poloidal magnetic fields [12].

Up to this moment, the confinement process of the fusion plasma has not been fully realized despite the intense study on the confinement modalities. The primary role of the plasma facing components (PFC) that are in the vicinity of the fusion plasma is to intake the generated heat and transfer it further at a higher rate [11].

Plasma-wall interactions can occur during the fusion plasma ignition. Therefore, the PFC can make contact with the resultant particle flux after the plasma fusion process. Plasma instabilities can cause important morphological changes at the level of the PFC and also at the level of the ignition, maintaining the fusion reaction cycle. As a result, the sputtered PFC can contaminate the plasma with material impurities, resulting in the contamination and shutdown of the fusion process [6].

The primary problem of a fusion working facility is presented by the erosion of the PFC as a result of the bombardment of the charged particles by neutrons that are highly energetic. A complex study regarding the processes that occur inside the reaction chamber by means of witness samples analyses that provide data on the

erosion or re-deposition degree is necessary. The witness samples are integrated into the fusion reactor as part of PFC. For example, the witness samples can be represented by the Be tiles deposited with Ni, Mo or W thin layers, respectively, or the W bulk state deposited with Mo-W alloys [12].

The interaction between the plasma and the components that are in the vicinity of it inside the reactor lead to the definition of the parameters for choosing the material that can be integrated into the future reactor vessel wall.

The materials have to:

- withstand high neutron fluxes at their surface (1 MW/m^2);
- present characteristics such as thermal fluctuations;
- perform erosion resistance;
- not react to plasma formed species in order to avoid volatile species;
- be good thermal conductors such as (C);
- form neutron irradiation species with a short lifetime [13].

Up to this moment, the research community had not successfully identified a complex alloy material that would meet all the above mentioned conditions; therefore, a combination of the most suitable materials is proposed to be integrated into the fusion reactor walls, taking into account the interaction yield with the plasma [14].

An important step towards the fusion energy production is taken through the optimization of materials that are in the near vicinity of the confined plasma in order to reduce the formation of radioactive waste, resulting in the reduction of the erosion, re-deposition and melting processes on the PFC elements [14].

From the past experimental campaigns, it was proven that the W element has the lowest erosion degree on interaction with the fusion plasma [15]. Nuclear fuel retention is low in the W integrated alloys, resulting in a high interest directed towards W element studies oriented towards plasma-wall interactions. As shown in Table 2.1, the W has the highest melting point when compared to other elements that are used in the fusion reactors, proving that it is a well-suited material for the divertor area, which is the inferior part of the reactor that is also the most exposed part inside the reactor chamber.

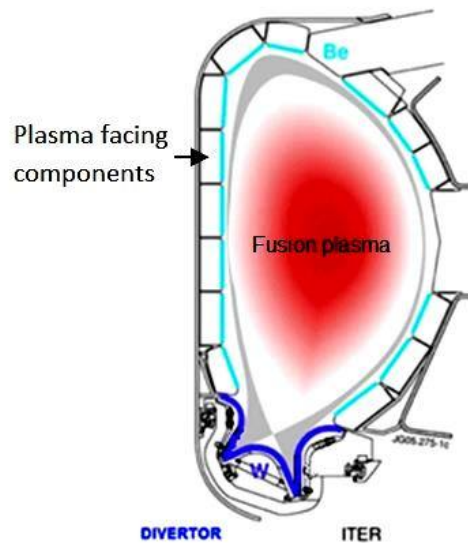
The PFC used for the JET reactor were realized from massive tiles of Inconel (alloy of Ni, Cr) with Be depositions on a massive substrate of C fibre composite (CFC), CFC deposited with W and in the divertor are W massive plates [16].

The W material is important and present in the Axially Symmetric Divertor Experiment-Upgrade (ASDEX Upgrade) reactor that is the only reactor that works with a metallic W wall.

Table 2.1 Relevant parameters for the most used materials in the fusion reactors [13]

Characteristics	W (Z=183.85)	Be (Z=9.01)	C / CFC (Z=12.011)
			fibre reinforced carbon composites (CFC)
Advantages	Minimum erosion and retention of nuclear fuel;	Low atomic mass;	Shock resistant;
Limitations	High atomic mass, reactive (the production of volatile species)	Melting;	High nuclear fuel retention, chemical erosion;
Thermal conductivity [W/m·K]	140	190	200 – 500
Melting point [K]	~3695	~1560	~2500
In relation with neutron interaction	reactive;	Volume expansion;	Thermal conductivity decrease;

Another example of the W implementation is for the ITER fusion facility that is under construction at Cadarache, France, wherein the first wall of the torus is intended to primarily integrate Be, W and Inconel materials (Figure 2.2.2).

**Fig. 2.2.2** Poloidal cross section (ITER) [18];

Initially, the future ITER reactor was designed with a reaction chamber deposited with Be (700 m²), while materials such as W (120 m²) and CFC (35 m²) could be used only in the divertor area [17]. Later studies provided information about the use of CFC, as PFC presents a high and rapid potential of T retention by means of co-deposition processes. Studies were conducted taking into account the vulnerable area inside the reactors torus, resulting in a determination of a high vulnerability area as a result of the presence of a high interaction yield during the fusion plasma discharge.

It is believed that after the ITER reactor becomes fully functional, studies conducted involving it will have a direct impact on future reactors such as DEMO (DEMONstration Power Station), which will be built based on the accumulated theoretical and experimental experiences in order to produce commercially available energy.

Hence, in order to make fusion energy available at a commercial scale, a complex program of testing of fusion relevant materials is needed. The fusion research programme on PFC involves many studies, technology validations and prototype development for fusion plasma relevant materials.

Over the last few years, due to the importance of involved processes that could occur in the near vicinity of the PFC in the study, different combination of materials has been proposed as witness samples. For example, in the NILPRP institute, deposition multilayers on bulk material tiles were fabricated from bulk Be deposited with thin layers of Ni and Be or bulk W deposited with Mo and W [17].

Chapter 3. Applied analysis methods

In **Chapter 3**, the working principles of the applied techniques, methods that are currently in use at the institute, such as Glow Discharge Optical Emission Spectroscopy (GDOES), Scanning electron Microscope (SEM) and Rutherford back-scattering spectroscopy (RBS), are elaborated. Furthermore, the X-ray fluorescence-based procedures, which are integrated into the micro tomography and image processing laboratory, are detailed.

The high diversity of materials that are included in the composition of the PFC was studied for its complex morphological and compositional modifications produced by means of different plasma-wall interactions. Therefore, a wide variety of analysing methods were applied on the non-exposed and exposed relevant samples.

In the subsection of this chapter, the principles of the complementary applied methods are briefly presented (Table 3.1). The presented investigation techniques were applied for comparative studies and reciprocal validations. The proposed complementary methods were Glow Discharge Optical Emission Spectroscopy (GDOES), Scanning Electron Microscope (SEM) and Rutherford Backscattering Spectrometry (RBS).

Table 3.1 Relevant samples used in the fusion technology, characterised by means of different analysis techniques.

Deposited samples (deposition method)	Fusion plasma exposure	Analysis methods	Output results
W/C, W/Si (TVA)	No	XRF	XRF calibration curve
Ni/C, Ni/Si, Ni/Glass (TVA)	No	XRF	
W+Mo/Ti (CMSII)	No	HEXRF	HEXRF calibration curve
Fe+Ni+W/Si (TVA)	No	XRF	Determination of spatial distribution of TVA deposited samples
Be+C+W/Si (TVA)	No	XRF, RBS	W deposition distribution

Exposed samples (2011-2012)	Exposed	XRF, HEXRF	Fe, Ni, Cr, W element determination
Witness samples W+Mo/Ti (CMSII)	No	GDOES, SEM, XRF	Standard samples for marker lamellae
Marker lamellae W+Mo/W (CMSII)	No	XRF, RBS	Before and after exposure study
Marker lamellae W+Mo/W (CMSII)	Exposed	XRF, RBS	

Due to each method's particular limitation, the application of a wide diversity of investigation methods is conducted. Thus, the methods present limitations based on resolution, sensibility and detectability interval. Therefore, no other analysis technique will be suitable for satisfying a full sample characterisation.

It is proposed that by means of multiple analysis methods, the investigations conducted will help define an ideal and robust material to be applied as PFC in future reactors. The majority of applied alternative methods were developed and are present in the NILPRP.

3.1 Alternative analysis methods

Subchapter 3.1 contains a short presentation of the applied methods in the current work, through which comparative studies were conducted. These methods need calibration samples and are destructive for the investigated sample surface.

3.1.1 Glow discharge optical emission spectroscopy method

The glow discharge optical emission spectroscopy (GDOES) is an alternative and sample destructive method that is capable of in-depth chemical composition, starting from a few hundreds of nanometre up to micrometre. The GDOES method is a fast method suitable for a quantitative analysis of thick metallic and non-metallic materials [20, 21].

The principle of the GDOES is presented in Figure 3.1.1. The samples that are analysed have contact with the cathode. The chamber where the glow discharge takes place contains Ar at a low pressure ($0.5 - 10 \times 10^2$ Pa). Due to a high applied voltage, the electrons are extracted from the surface of the sample and are accelerated towards the anode, finally gaining kinetic energy [22].

By inelastic scattering, the electrons transfer their kinetic energy to the Ar atoms, forming Ar positive ions and other electrons. Therefore, the density of the charge carrying particles rises and results in a conductive gas (Figure 3.1.1).

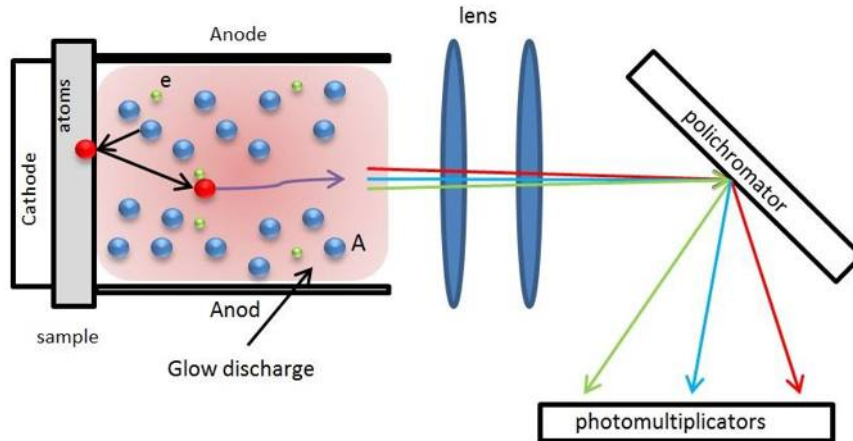


Fig. 3.1.1 Working principle of the GDOES method

Thus, the plasma is formed by a mixture of Ar atoms and free charge particles (Ar ions and electrons). Positive ions of Ar are accelerated towards the sample surface by means of potential difference. The ions that directly hit the sample surface remove the sample atoms by means of scattering effects, resulting in the erosion of the sample surface [22].

The extracted atoms from the sample surface interact with the highly energetic electrons present in the plasma. During these collisions, energy is transferred to the sample atoms in order to maintain their excitation state. During the de-excitation, atoms emit photons with a characteristic wavelength.

In the current work, in order to realise the GDOES measurements, it applied the *GDA750* instrument produced by *Spectruma*. This instrument can conduct in-depth analysis up to 200 μm , with a detection thickness of nanometre range.

3.1.2 Scanning electron microscope method

The scanning electron microscope (SEM) method determines the morphology images, not in-depth but on the sample surface. The samples that are intended to be analysed by means of SEM method have to be prepared in order to face vacuum conditions and high energy electron fluxes, thus avoiding the image defocussing during the measurements.

The SEM working principle is based on the measuring of the scattered or emitted electron fluxes from the sample surface. Therefore a narrow flux of electrons is scanned on the surface of the samples and a high number of dispersed electrons are translated to a sharp image. Particularly, for the current applied work, the SEM method produces high resolution images with up to 1 nm resolution.

The electron beam generator tube has the W cathode as target component, thus facilitating the thermo-emission of electrons. The electron beam with an energy interval starting from 0.2 keV up to 40 keV is focalized by means of a concentrator lens with an aperture of nanometre region. The beam passes through these collimators

and is deviated with the help of deflection plates, in order for the electron beam to be scanned on the X and Y axis.

When the primary beam interacts with the sample, the electrons lose their energy through the different processes of scattering and absorption that takes place into the so-called interaction volume. This interaction volume is strictly dependent on the sample density, on the atomic number and the incident electron energy. The interaction between the electron fascicle and the samples results in high energy scattered electrons by means of elastic scattering, secondary electron emission by means of inelastic scattering and electromagnetic radiation emission. All these particular signals can be analysed by means of specially designed detectors.

In the current work, the applied SEM method relied on the detection of secondary electrons. Low energy secondary electrons (<50 eV) [23] that is a result of the exposure from the K-line of the investigated sample atoms are collected by means of inelastic interactions with the electron incident beam. Due to the low penetration of the incident electrons, those determine the formation of secondary electrons only at the surface of the sample. The electrons are detected thus by applying an Everhart-Thornley type detector represented by a system that includes scintillators and photo-multipliers [24].

If the incident angle between the sample and the focussed beam is enhanced, it will result in a bigger interaction volume, thus leading to a higher number of secondary electrons on the sample surface. Therefore, the edge of the samples and areas with distinct morphology will appear as brighter, resulting in well-defined and focalized images.

3.1.3 Rutherford backscattering method

The Rutherford backscattering spectrometry method (RBS) represents a nuclear method applied usually on solid surface investigation. This method permits a depth composition determination based on the studied samples. This is applied in the determination of the structure and composition of materials by means of a scattered beam of ions at high energies (protons and alfa particles). Generally, this method is applied for multilayer sample investigation or on samples with a constant variation of in depth composition.

The appliance of this method avoids the use of standard samples, is non-destructive, has a good in depth resolution up to few nanometres and represents a good sensitivity for high Z elements. The analysed depth depends strictly on if the target is bombarded with He ions (2 μm) or protons (20 μm) [25]. This method has a disadvantage for the determination of light elements.

The methods working principle stands on the ion bombardment of a target with energies in the MeV region, while the energy of scattered particles is measured by means of a detector.

The energy loss of the back-scattered ions are the result of scattering incidents that take place at the sample nucleus level and low angle scattering that involves sample electrons

The first mentioned process depends on the nucleus scattering cross section in relation to their mass and atomic number. At a well-defined angle, two different

element nuclei will scatter ions at different angles and energies. These differences that appear in the spectra as intensity peaks are assigned to each element contained in the material. Therefore, the composition measurement by means of scattering energy identification is favoured, and the relative concentration could be determined by the intensity of the characteristic lines.

The second process of energy loss stands in the breaking capacity of electrons inside the sample, although no discrete spectra could be observed. Meanwhile, energy loss can happen as a result of the electron density and the distance travelled in the sample.

Therefore, the measured ions that were previously back-scattered by means of interactions that involves sample nucleus have their energy diminished in a continuous and position-dependent manner.

Thus, well defined intensity peaks are not present; characteristic peaks are localized at lower energies while the ions pass through the sample depth where the element is present. Elements that exist in the depth of samples will appear with the positions of the intensity peaks shifted in the spectra in relation to the distance that the ions have to travel before reaching the respective nucleus.

Hence, the compositional depth profile could be determined by means of RBS, which studies the positions of the intensity peaks in the spectra. The depth at which the elements in the sample are present could be determined by the position of the intensity peaks and their length.

3.2 Non-destructive methods

From the physical process point of view, the X-ray fluorescence represents the emission of characteristic energetic lines from a material that was excited by means of high energy X-rays. This method helps in the identification of elements in the sample and measuring their concentration in a non-destructive and fast manner.

In the past, many applications for the X-ray fluorescence based methods could be observed. Depending on the nature of the investigated material, such as metals, alloys, glass, minerals, rocks, polymers, elements that are present in varied concentrations could be determined selectively.

By applying X-ray fluorescence based methods (XRF), one can analyse low atomic elements starting from Na, up to higher atomic number elements as U. Instead, for the identification of light elements, such as Be, the X-ray energy dispersive spectroscopy (EDS) could be an alternative. This method is based on the use of an electrons beam with low penetration in the analysed sampled depth, thus becoming an advantage of studying PFC samples.

Sample preparation is crucial for a better determination of the elemental concentration in a sample. This process could vary from a simple sample surface cleaning up to the polishing of the surface that could be made of pure metals or alloys up to treatments with acids. Therefore, errors than can occur due to the surface roughness could be mitigated.

In the current work, the primary methods applied for investigating the surfaces relevant to the fusion domains were those based on the generation of X-ray

fluorescence at low (micro-XRF) and high energies (HEXRF). These were developed in-house at the micro-tomography and image processing laboratory from the NILPRP.

These methods are already applied in various domains where a non-destructive and rapid investigation is needed, such as for the metallic depositions on large areas, resistant layers at high temperatures and functional materials with applicability in the industrial domain. Additionally, these methods are used simultaneously in the determination of layer composition and thickness in the electronic industry and other vast technological areas [26].

By means of applying methods based on the X-ray fluorescence, one can determinate the thickness of material layers for tens of nanometres up to hundreds of micrometre in alloy or multilayer configurations [27].

The XRF method integrates into its instrument configuration the following components: X-ray source, energy selective detectors, optical concentrators for X-ray beam, collimators and translational motorized axis. By means of motorized axis, mappings of large area surfaces are possible. All XRF protocols are presented in the following subchapters (3.2.1.–3.2.4).

3.2.1. X-ray sources

X-rays are electromagnetic fields with a wavelength starting from 1 eV up to MeV range. The electromagnetic radiations (over 1 MeV) are generated in the nuclear process and are named gamma radiation [31]. The generation of X-rays is explained as a spontaneous disintegration of certain isotopes and by means of the interaction between the artificially accelerated electrons with the anticathode material.

In an X-ray tube, the electrons that are emitted from the cathode are accelerated towards the anode by means of a potential difference. The accelerated electron hits the target's material and interacts with its atoms, resulting in a loss of energy by means of several processes.

Only a small fraction of incident electrons are inelastically scattered, thus decelerating in a Coulomb field and gradually losing their energy. Therefore, the result is a continuum and decelerated spectra, named 'Bremsstrahlung' [28].

Secondly, the incident electrons that interact with the target's electrons transfer their energy. The primary process consists of a successive collision with other electrons, thus producing only a small energy loss. In particular cases, one electron could be removed from the atom's orbit, determining an ionized atom. Sometimes, other electrons can fill the vacancy in the orbital, and the energy excess is freed as X-ray quantum. In this manner, the characteristic X-ray lines are made present in the emitted spectrum. Figure 3.2.1 shows the characteristic lines presented for a W target X-ray source working at different voltage parameters.

Every spectrum is made from a discrete and a continuum part. The shape, intensity and maximum energy of continuum spectrum is dependent on the applied voltage on electrodes, while the discrete line positions are based on the material from which the target is made of.

The apparition of a specific characteristic line depends on the acceleration voltage applied on the source. Therefore, the characteristic lines in spectra will not